7-4-2023

Naturally occurring highly pathogenic avian influenza virus H5N1 clade 2.3.4.4b infection in three domestic cats in North America during 2023

Sarah J. Sillman

Mary Drozd

Duan S. Loy

Seth P. Harris

Journal of Comparative Pathology 205 (2023) 17–23

Contents lists available at ScienceDirect

Journal of Comparative Pathology

journal homepage: www.elsevier.com/locate/jcpa

Infectious disease

Naturally occurring highly pathogenic avian influenza virus H5N1 clade 2.3.4.4b infection in three domestic cats in North America during 2023

Sarah J. Sillman*, Mary Drozd, Duan Loy, Seth P. Harris

Nebraska Veterinary Diagnostic Center, School of Veterinary Medicine and Biomedical Sciences, University of Nebraska-Lincoln, 4040 East Campus Loop North, Lincoln, Nebraska 68583-0907, USA

ARTICLE INFO

Article history:
Received 19 May 2023
Accepted 4 July 2023

Keywords:
cats
encephalitis
highly pathogenic avian influenza virus
vasculitis

ABSTRACT

The Eurasian strain of highly pathogenic avian influenza (HPAI) H5N1 is a devastating pathogen for birds that also has the capacity to infect mammals. This report describes the presentation, clinical case findings (including haemogram and serum biochemistry), gross and microscopic lesions and virus detection in three HPAI H5N1-infected domestic cats from the USA in 2023. All three cats presented with neurological abnormalities and were euthanized due to a poor prognosis within 2 days (two cats) or 10 days (one cat) of known clinical disease onset. Necropsy consistently revealed pulmonary congestion and oedema, and cerebrocortical malacia with haemorrhage was also seen in the cat that survived for 10 days. On histology, all cats had necrotizing encephalitis and interstitial pneumonia with pulmonary congestion, oedema, vasculitis and vascular thrombosis. One cat also had microscopic multifocal necrosis in the liver, pancreas and an adrenal gland. To our knowledge, this report is the first to detail pathological findings in HPAI H5N1 naturally-infected cats during the widespread outbreak in North America beginning in 2021, and that describes a cat surviving for 10 days after onset of HPAI H5N1 encephalitis.

In late 2021, the Eurasian strain of highly pathogenic avian influenza (HPAI) H5N1 was detected in North America, initiating an outbreak that continues into 2023 and that has affected at least 60 million commercial and wild birds in the USA [1,2]. Spillover infections of HPAI H5N1 occur in both terrestrial and marine mammals [3]. During previous avian influenza pandemics with H5N1 (A/swan/Germany/R65/06) in 2006 and with H5N6 (A/feline/Korea/H646/2016) in 2016, domestic cats were naturally susceptible to H5 HPAI strains [4,5]. These viruses have temporal and phylogenetic differences compared with the current HPAI H5N1 virus of the goose/Guangdong lineage, clade 2.3.4.4, that has been circulating in the USA since 2021 [6]. Therefore, there is a need to continue examining these domestic cat spillover infections, particularly given that cats live in close proximity to humans and theoretically have a role in influenza virus transmission [7]. Natural and experimental H5 HPAI infections of cats have resulted in various combinations of lesions, including multifocal hepatic and adrenal gland necrosis, conjunctivitis, encephalitis and/or pneumonia [5,8–10]. However, reports of feline lesions associated with the current HPAI strain predominantly circulating in North America (Eurasian H5 clade 2.3.4.4b with North American lineage segments) are limited and the variety of clinical and pathology case presentations for infected cats has not been fully described. This report describes the case presentations, haemogram and serum biochemistry findings, gross and microscopic lesions and HPAI H5N1 virus detection in three domestic cats in Nebraska, USA, which were naturally infected during the recent North American outbreak of H5N1 among wild and domestic poultry. The report highlights the primary lesions of the infection and describes the variation of lesions associated with the duration of disease.

In January 2023, a 2-year-old, male neutered, Domestic Shorthaired cat (case 1) was presented to a Northeast Nebraska veterinary clinic as non-ambulatory and anorectic. The cat was kept outdoors and had been missing for a few days prior to being found in an abnormal state. Three other free-roaming, outdoor cats were housed on the premises. Physical examination documented anisocoria, injected sclera, nystagmus, loss of proprioception, tremors, hyperesthesia, pyrexia (body temperature 40.6°C; reference interval [RI] 36.7–38.9°C) and an elevated respiratory rate of 70 breaths per minute (RI 15–42 breaths per minute). Blood glucose was

* Corresponding author.
E-mail address: sarah.vitosh@unl.edu (S.J. Sillman).

https://doi.org/10.1016/j.jcpa.2023.07.001

200 mg/dl (RI 80–120 mg/dl). The cat received treatment with dexamethasone, ampicillin, gentamycin, maropitant and lactated Ringer's solution (LRS) intravenous fluid therapy. The following day, the cat had a series of five seizure episodes despite administration of diazepam and was euthanized due to its deteriorating condition.

On necropsy, the lungs were diffusely and moderately congested and oedematous, and there was mild pericardial transudative effusion. Distinctive, random, darker grey patches interspersed with areas of normal colouration subtly mottled the cerebral cortical grey matter. Representative samples of heart, trachea, oesophagus, lung, spleen, liver, adrenal gland, skeletal muscle, mesenteric lymph node, pancreas, stomach, small and large intestines, kidney and brain were fixed in 10% neutral buffered formalin and processed for routine histopathological examination with haematoxylin and eosin (HE) staining.

Microscopically, lesions were prominent in lung and brain, but also involved multiple visceral organs. Lung sections had severe, diffuse pulmonary oedema and vascular congestion associated with patchy areas of mild interstitial pneumonia and vasculitis. The interstitial pneumonia was characterized by expansion of the alveolar walls by loose to aggregated fibrin occasionally associated with a few macrophages and neutrophils. Occasional vascular walls had fibrinoid necrosis, invasion by small numbers of mixed leucocytes and/or lumina occluded by fibrin thrombi (Fig. 1A). The bronchiolar epithelium was often partially denuded, and autolytic to acutely degenerative epithelial cells were exfoliated into the airways admixed with oedema fluid and mucus.

Sections of cerebral cortex, cerebellum, brainstem and hippocampus had meningoencephalitis with characteristic wedge-shaped and laminar areas of necrosis centered on the cerebral cortical grey matter, hippocampus and brainstem nuclei (Fig. 2A) that were associated with vasculitis. The vasculitis varied from vessel walls partially obscured by neutrophils, lymphocytes and/or karyorrhectic debris to occasional fibrinoid necrosis (Fig. 2B). Wedge-shaped areas of necrosis contained scattered or aggregated groups of necrotic neurons characterized by increased angularity and cytoplasmic

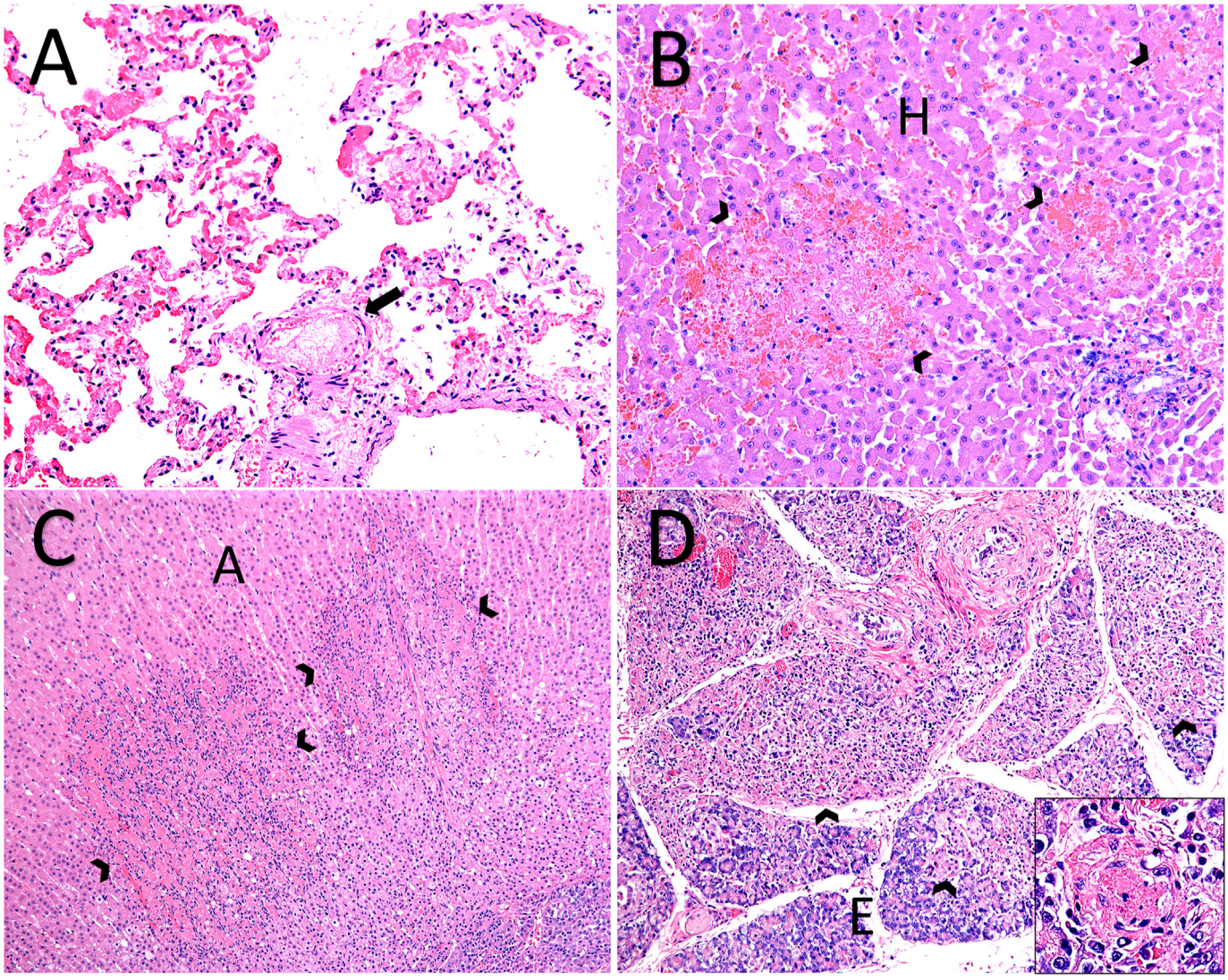

Fig. 1. Highly pathogenic avian influenza virus H5N1 infection, cat, case 1. (**A**) Lung. Interstitial pneumonia characterized by acute vascular congestion, alveolar oedema and exudation of fibrin mixed with few neutrophils and macrophages into the alveolar septa and lumina. Thrombosis (arrow). HE. ×400. (**B**) Liver. Multifocal, variably sized, random foci of acute necrosis (arrowheads). Necrotic areas contain fibrin, karyorrhectic debris, erythrocytes and sparse neutrophils and/or macrophages. Region of normal hepatocytes denoted for comparison (H). HE. ×200. (**C**) Adrenal cortex. Large foci of random acute necrosis (arrowheads). Region of normal adrenal cortical cells denoted for comparison (A). HE. ×100. (**D**) Pancreas. Severe, multifocal to coalescing necrosis manifesting as extensive loss of pancreatic exocrine cells and collapse of lobules (arrowheads). Mixture of inflammatory leucocytes and karyorrhectic debris can be found in the remnant stroma. Region of normal pancreatic exocrine cells denoted for comparison (E). HE. ×100. Inset: several vessels observed in pancreas with endothelial necrosis, fibrinoid change and thrombosis.

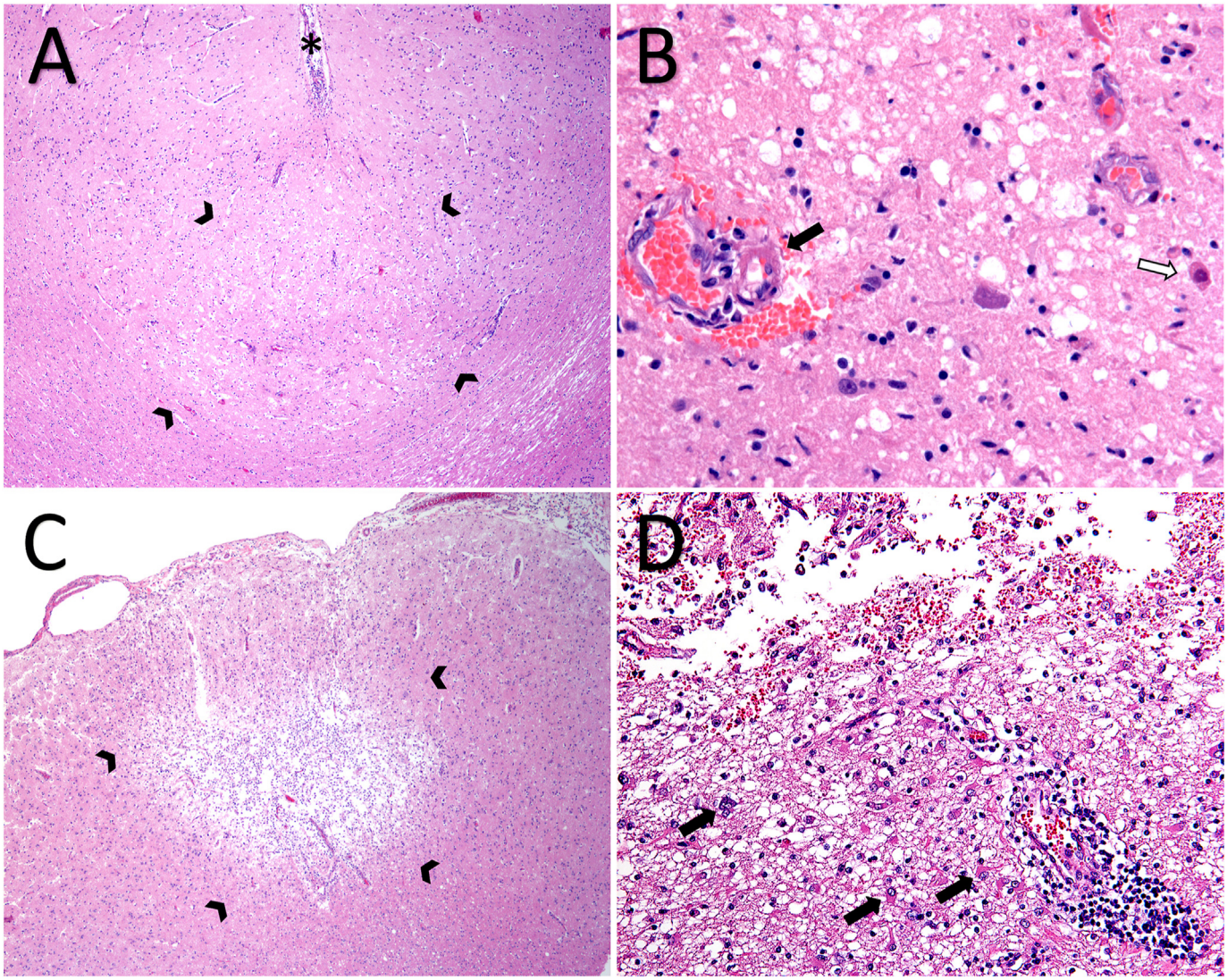

Fig. 2. Highly pathogenic avian influenza virus H5N1 infection, cats. (**A**) Brain, cerebral cortex, case 1. Wedge-shaped area of necrosis with spongiosis (outlined by arrowheads). Sulcus (*). Scant lymphocytes, macrophages and neutrophils in meningeal space above necrotic focus. HE. ×40. (**B**) Brain, brainstem, case 1. Vasculitis with necrosis and fibrinoid change (black arrow). Spongiosis and necrotic neurons (white arrow). HE. ×400. (**C**) Brain, cerebral cortex, case 2. Wedge-shaped area of necrosis with malacia and cavitation (outlined by arrowheads). HE. ×40. (**D**) Brain, cerebral cortex, case 2. Clefted area containing erythrocytes, neutrophils, macrophages and fibrin at border of malacic area. Surrounding neuropil is spongiotic, containing gemistocytic astrocytes (arrows). Mononuclear cell perivascular cuffing present. HE. ×200.

eosinophilia and nuclear pyknosis. The adjacent neuropil had mild to moderate spongiosis and scattered karyorrhectic fragments, gitter cells, spheroids, neutrophils infiltrating the parenchyma and rare glial nodules. There were small, sparse foci of Purkinje cell necrosis with spongiosis in the cerebellar cortex, but most of the cerebellum was unaffected. The leptomeninges had mild, lymphohistiocytic and neutrophilic inflammation that extended into Virchow–Robin spaces.

The liver (Fig. 1B), adrenal gland (Fig. 1C) and exocrine pancreas (Fig. 1D) had small to medium sized, random areas of acute necrosis with small amounts of suppurative to histiocytic inflammation. The necrotic foci were well circumscribed and associated with karyorrhectic debris and mild exudation of fibrin, pyknotic endothelial cells and vascular thrombosis. The pancreas had additional mild, interstitial, lymphoplasmacytic inflammation that was considered an unrelated finding. Occasional blood vessels in the pancreas and other organs, including the heart and intestinal tract, had minimal to mild transmural degeneration of small blood vessels. Lymphoid tissues within spleen, mesenteric lymph node and intestinal tract had mild lymphoid depletion. In mesenteric lymph node, the medullary sinuses contained moderate amounts of fibrin admixed with macrophages and neutrophils. Within one representative section of kidney there were small groups of cortical tubular epithelial cells that had acute coagulative necrosis without inflammation.

Approximately 24 h after presentation of case 1, another cat from the same residence, an 8-month-old, spayed female, Domestic Long-haired cat (case 2), became somnolescent and walked in circles. Haemogram and serum biochemistry were performed on initial presentation, and there was mild hyperalbuminaemia (Supplementary Table 1). The cat was responsive to stimuli and was observed eating and drinking. For suspected toxicant exposure, activated charcoal was administered by mouth, and daily treatment thereafter consisted of LRS intravenous fluid therapy, dexamethasone and maropitant. This cat survived for 10 days with stable neurological signs, after which it suddenly became laterally recumbent with continual tremors. The cat was euthanized due to a poor prognosis.

On necropsy, this cat was slightly underweight with moderate muscle atrophy. There was a small amount of crusted, bloody fluid around the nostrils. All lung lobes were diffusely congested.

During the process of brain removal, approximately 20 ml of bloody cerebrospinal fluid exuded from the foramen magnum. Along the left cerebral cortex, most severely affecting the occipital and temporal lobes, there was a poorly demarcated region of malacia with focal haemorrhage. The friable, softened gyri were distinctively light yellow (Fig. 3A). On cross-section, the haemorrhagic focus was an area of parenchymal fragmentation and clefting with haemorrhage (Fig. 3B). Representative samples of nasal turbinate, tonsil, pituitary gland, urinary bladder, kidney, heart, trachea, oesophagus, lung, spleen, liver, adrenal gland, skeletal muscle, mesenteric lymph node, pancreas, stomach, small intestine, colon and brain were fixed in 10% neutral buffered formalin and processed for routine histopathological examination with HE staining.

Microscopically, the cerebral cortex had wedge-shaped to laminar areas of malacia with variable rarefaction, cavitation and haemorrhage (Fig. 2C). These areas had extensive loss of neuropil; the tissue was friable and fragmented during sectioning. The rarified parenchyma consisted of a network of supporting small blood vessels among scant, fragmented neuropil with extensive neuronal loss and infiltration by abundant gitter cells and astrocytes admixed with fewer neutrophils, lymphocytes and variable numbers of erythrocytes (Fig. 2D). Numerous gemistocytic astrocytes were spread throughout the cortex and were most dense around foci of malacia. There were occasional, small to moderately sized, mononuclear perivascular cuffs throughout the brain, which were prominent near malacic areas with minimal to mild cuffing within the cerebellum and brainstem. The brainstem and cerebellar meninges contained few lymphocytes and macrophages. There was an occasional digestion chamber in the brainstem white matter. The lung had interstitial pneumonia similar to case 1, with the addition of more macrophages populating the alveolar septa, less overt vascular thrombosis and a few foci of mild type II pneumocyte hyperplasia. The myocardial interstitium contained a few random clusters of lymphocytes.

In April 2023, a 6-month-old, female spayed, Domestic Shorthaired cat (case 3) was presented to a veterinary clinic in Central Nebraska for difficulty ambulating, lethargy and anorexia. This animal resided outdoors and was one of nine cats on the premises. On physical examination, there was moderate mucoid discharge from the nares and body temperature was 39.5°C (RI 36.7–38.9°C). Haemogram was within normal limits. Serum biochemistry revealed only mild abnormalities, namely hyperglycaemia, decreased blood urea nitrogen and creatinine, hyperproteinaemia, hyperglobulinaemia, hyperbilirubinaemia and hyperlipasaemia (Supplementary Table 1). Despite supportive treatment with metronidazole, amoxicillin-clavulanic acid, emodepside/praziquantel topical, atropine and subcutaneous fluid therapy, the cat continued to decline and it was euthanized 1 day after presentation. In a 2-week period around this case, four additional cats died at the premises but were not available for post-mortem evaluation.

On necropsy of case 3, all lung lobes were mottled red with patchy atelectasis or overinflation. Severe pulmonary oedema was seen on cut section. Representative samples of thyroid gland, urinary bladder, bone marrow, kidney, heart, trachea, oesophagus, multiple lung lobes, spleen, liver, skeletal muscle, lymph node, pancreas, stomach, small and large intestines and brain were fixed in 10% neutral buffered formalin and processed for routine histopathological examination with HE staining.

Histologically, the brain lesions were similar to cases 1 and 2 with wedge-shaped areas of inflammation most commonly located within the cerebral cortex. However, areas of glial and mononuclear cell inflammation with mixed lymphocytes, plasma cells and macrophages were more extensive and numerous than seen in previous cases and often had more abundant cellular debris, degenerate neurons and glial cells and neuronal satellitosis (Figs. 4A and C). Inflammatory cell cuffs comprised of lymphocytes, plasma cells, macrophages and neutrophils expanded Virchow–Robin spaces, and more severely affected vessels had leucocyte invasion into the vascular wall, scant amounts of fibrinoid necrosis and endothelial cell necrosis (Fig. 4B). The adjacent neuropil had moderate spongiosis with moderate gliosis and scattered, acutely necrotic neurons. In the lungs, the distal airways contained abundant, proteinaceous oedema fluid admixed with loosely arranged fibrin (Fig. 4D) and alveolar septa were obscured by fibrin thrombi or mildly thickened by pneumocyte hypertrophy.

Tissues and swabs from the three cases were processed for quantitative real-time polymerase chain reaction (qRT-PCR) to determine the presence or absence of the Eurasian H5 strain of HPAI following protocols provided by the US Department of Agriculture National Animal Health Laboratory Network (USDA NAHLN). RNA was extracted as described using the MagMAX 96 Viral RNA Isolation Kit (AM 1836; Applied Biosystems, www.thermofisher.com) with the KingFisher Flex Magnetic Particle Processor (Thermo Fisher Scientific, www.thermofisher.com). Quantitative reverse transcription real-time polymerase chain

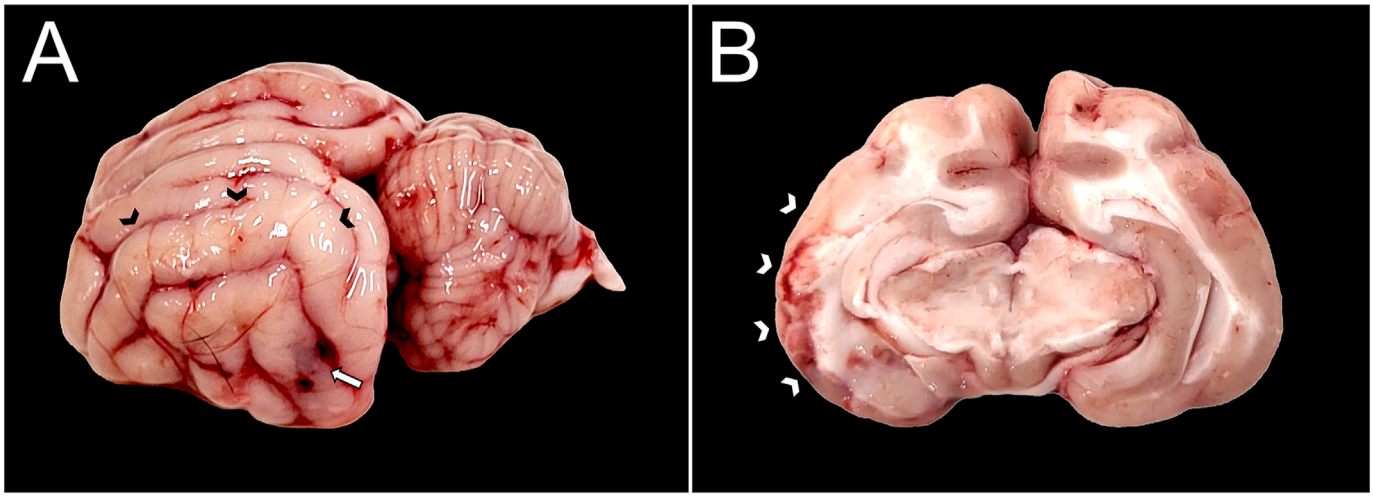

Fig. 3. Highly pathogenic avian influenza virus H5N1 infection, cat, case 2. (**A**) Left cerebral hemisphere and cerebellum. Distinctive area of malacia marked by yellow discolouration (outlined by arrowheads) and a well-demarcated red, haemorrhagic focus (arrow). (**B**) Cross-section of brain at level of haemorrhagic focus with transected area of malacia with neuropil fragmentation, clefting and haemorrhage (demarcated by arrowheads).

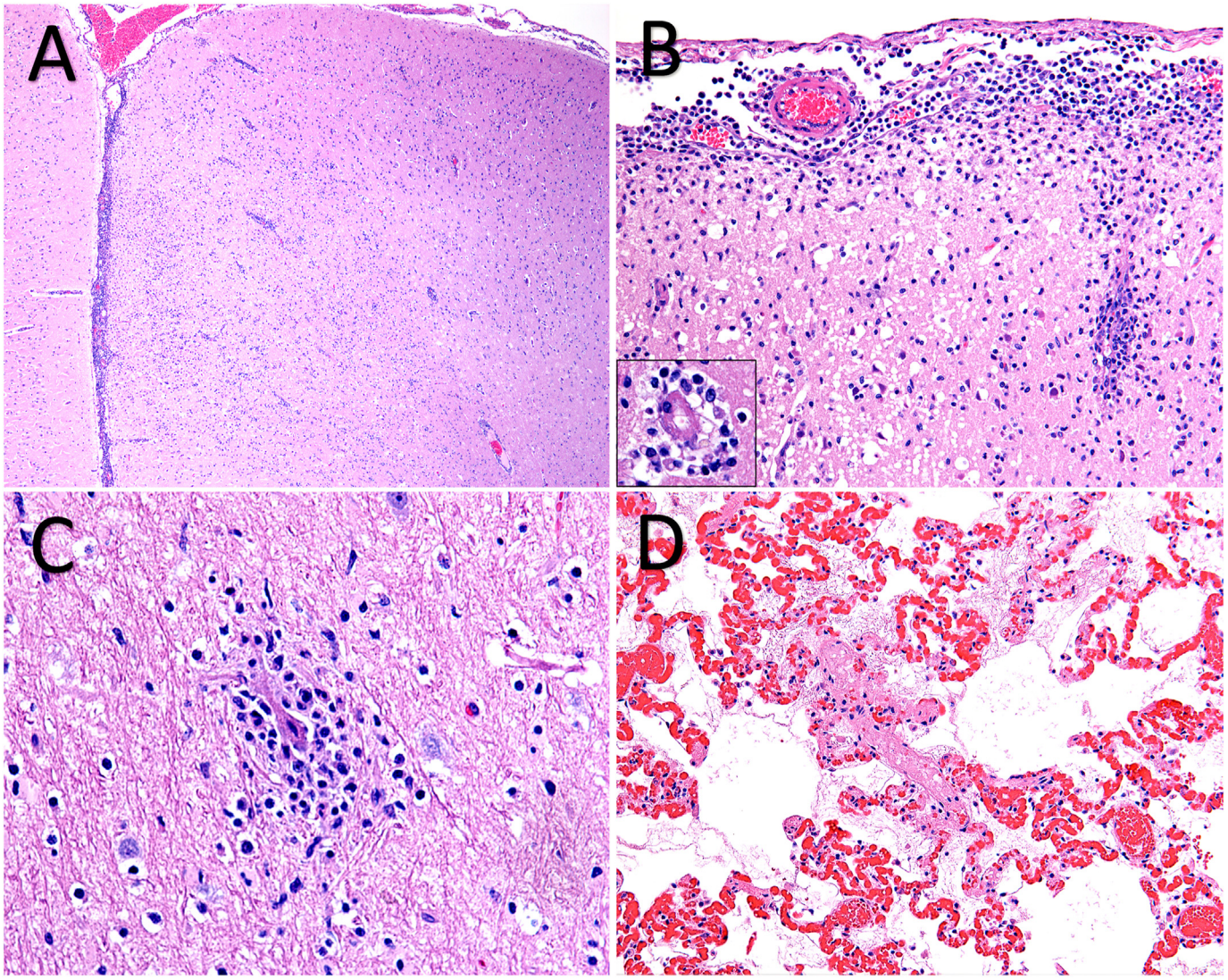

Fig. 4. Highly pathogenic avian influenza virus H5N1 infection, cat, case 3. (**A**) Brain, cerebral cortex. Discrete, wedge-shaped area of inflammation with associated neuronal necrosis. HE. ×40. (**B**) Brain at higher magnification. Cerebral cortical lymphohistiocytic inflammation involving meninges and perivascular regions. HE. ×200. Inset: associated spongiosis, neuronal necrosis, gliosis and fibrinoid vasculitis. (**C**) Brainstem. Localized gliosis and neuronal satellitosis. HE. ×400. (**D**) Lung. Interstitial pneumonia with focally extensive vascular thrombosis, localized vascular congestion and fibrin exudation. HE. ×200.

reaction (rRT-PCR), which targets the influenza M gene 14, was performed using the 7500 FAST Real-time PCR System (Applied Biosystems) and H5 AM/EA 2014 and the AgPath-ID OneStep RT-PCR Reagents (Applied Biosystems) according to the USDA National Veterinary Services Laboratories (NVSL) protocol provided to USDA NAHLN laboratories. A cycle threshold value (Ct) of ≥45 was considered a negative result. For case 1, an acute presentation, rRT-PCR detected avian influenza (AI) virus and H5 subtype on brain (AI Ct 12.26, AI H5 Ct 12.38), a post-mortem deep nasal swab (AI Ct 35.30, AI H5 Ct 38.34) and liver (AI Ct 19.20, AI H5 Ct 19.87). A faecal sample from the cat was also tested, but AI was not detected. Nasal swabs were collected from the three living cats (case 2 cat and two clinically normal cats) 7 days after the death of case 1, and AI was not detected in these samples. For case 2, a chronic presentation, AI with H5 subtype was detected by PCR on brain (AI Ct 30.10, AI H5 Ct 31.31) and liver (AI Ct 33.90, AI H5 Ct 34.12). A deep nasal swab taken at necropsy did not detect AI. For case 3, an acute case, AI with H5 subtype was detected in the brain (AI Ct 17.88, AI H5 Ct 17.06). Non-negative samples were forwarded to the USDA NVSL and confirmed as Eurasian clade 2.3.4.4b H5N1 HPAI. A summary of the results is provided in Supplementary Table 2.

Immunohistochemistry for influenza virus A was performed on 4 μm sections of paraffin-embedded, formalin-fixed tissues previously evaluated and described with HE. The slides were deparaffinized and immunolabelled using an automated immunohistochemical stainer (Benchmark Ultra IHC/ISH System; Roche Diagnostics, https://diagnostics-roche.com). The primary antibody was a rabbit anti-influenza A virus nucleoprotein antibody (Invitrogen, www.thermofisher.com), used at 1:1000 dilution. Positive and negative controls for influenza virus labelling consisted of a slide containing known positive tissue (experimentally-infected animal lung) and slides of test samples treated with an irrelevant antibody (normal rabbit polyclonal immunoglobulin), respectively. After deparaffinization, the slides were incubated with a cell-conditioning solution at 95°C for 64 min, and primary antibody incubation was for 28 min with heat off. Secondary antibody incubation and immunolabelling were conducted with commercial reagents using the manufacturer's recommended protocols. Tissues were counter

stained with haematoxylin for 4 min, coverslipped and examined by light microscopy for immunoreactivity.

In case 1, there was rare positive immunolabelling in cardiac myocytes, renal medulla tubular epithelial cells, a sloughed cell in a bronchiole and adrenal chromaffin cells. There was occasional, multifocal immunolabelling of the adrenal cortical epithelial cells and cerebellar Purkinje cells and granule cells associated with areas of necrosis. Pancreatic exocrine and ductal epithelial cells and myenteric plexus ganglion cells of the small and large intestines had frequent, multifocal immunolabelling. There was frequent, multifocal to widespread, intense labelling of neurons and glial cells associated with areas of necrosis and inflammation in the brainstem, cerebral cortex and hippocampus.

In case 2, there was rare immunolabelling of cerebellar granule cells, cerebral cortex glial cells and sporadic cells in the malacic areas of vague morphology, which could have been gitter cells or degenerated neurons.

In case 3, there was rare labelling of medullary renal tubular epithelial cells. There was frequent, intense immunolabelling of neural tissue similar to case 1, but without virus antigen localization in Purkinje cells or the granule cell layer of the cerebellum.

Influenza A viruses were sequenced directly from samples and analysed as described [11]. Whole genome sequence data obtained for two of the three samples were consistent with reassortant viruses of the Eurasian H5 clade 2.3.4.4b with North American lineage segments. Partial sequence from case 1 was genetically similar to other virus sequences detected in wild birds in the upper Midwest of the USA during the spring of 2023. (The sequence from case 1 is deposited in GISAID [https://gisaid.org] as EPI_ISL_17821929.) A high-quality sequence obtained from case 3 was consistent with genotype B3.2, which has been the predominant genotype throughout the USA since August 2022. (The sequence from case 3 is deposited in GISAID [https://giasaid.org] as EPI_ISL_17821770.) Further sequencing attempts conducted on the samples from case 2 were unsuccessful.

The distribution of virus and lesions in other HPAI H5N1-infected cats has been described in natural cases and controlled experiments [4,5,8,10,12,13]. These reports detail a fulminant, highly fatal systemic disease with necrosis and inflammation in multiple organs and clinical signs primarily referrable to the respiratory and nervous systems. The hepatic, adrenal and pancreatic necrosis, pneumonia and encephalitis in the present cases were comparable to those lesions produced by prior circulating strains of H5N1. However, the vasculitis and vascular thrombosis in the three affected cats, particularly the acute cases, was distinctive and part of a discriminating pattern of tissues changes for HPAI H5N1 in domestic cats among these diagnostic cases. Although vasculitis has been mentioned in a prior report [8] and endothelial hypertrophy described in experimental infection [12], histological details of vascular abnormalities in feline infections are sparse. As HPAI H5N1 can cause massive infection of endothelial and lymphendothelial cells during systemic spread in intestinally-inoculated domestic cats, vascular disease may play a role in the pathogenesis [12]. For example, in case 1, overt vessel thrombosis was seen in the lungs, intestines, liver and pancreas, and variations of vasculitis were seen in organs, including fibrinoid and minimal leukocytoclastic changes. While foci of necrosis may be due to direct viral infection of parenchymal cells and neurons as demonstrated in prior studies characterizing the distribution of virus antigen [4,12], the wedge-shaped areas of necrosis throughout the cerebral cortex in these affected cats were suggestive of ischaemic injury from vascular damage as a contributing factor to disease. The oedema, fibrin exudation and thrombosis in the lungs of these cats were supportive of endothelial damage. The authors classified the histological pattern of lung injury in these cats as interstitial pneumonia but recognize that diffuse alveolar damage (DAD) is a histological pattern subtype that may result from direct damage to endothelial cells and for which influenza virus infections are a known cause [14]. In these three cats, the authors did not observe hyaline membranes along the surfaces of alveoli, a key feature of DAD [14]. Therefore, the fibrin exudation and subsequent histiocytic expansion (case 2) of alveolar septa was semantically reported as interstitial pneumonia. Experimental infection of cats intratracheally inoculated with H5N1 produced histological lesions of DAD, but the report did not detail the components of the lesion pattern [9]. Other reports of HPAI H5N1 lung lesions have varied from bronchointerstitial pneumonia, either uncomplicated or complicated with *Aelurostrongylus* sp. infection [4,10,13], to interstitial pneumonia of vague composition with capillary thrombosis and/or oedema and vascular congestion [5,8]. Therefore, this report adds clarity to the type of HPAI H5N1 lung lesions that occur in domestic cats with recent, uncomplicated infections under natural conditions.

Among these cases, brain was the best diagnostic sample, giving the lowest PCR Ct values when multiple sample types were tested. The samples of brain used for testing were from randomly selected areas. The authors propose that a random sample of cerebral cortex should be sufficient for testing, given the distribution of lesions observed and the abundant virus genome signal that was found at this location. Other organs, such as liver and lung, could be feasible diagnostic samples if brain is not available. Deep nasal swabs could be utilized for diagnosis if the disease is acute, but are unreliable if coverage of the nasal mucosa is inadequate or the cat has had clinical signs for several days, and certainly if for 7 days or more (case 2). Although it has been documented in experimental infection that cats may shed other strains of H5N1 rectally [13], faecal samples from the cat with high viral load and multiorgan lesions (case 1) did not have any detectable virus in faeces obtained from the rectum at necropsy. In support of the limited excretion and poor transmissibility of the virus to humans from infected cats, no human cases of H5N1 were documented in people in contact with these cats, including caretakers and veterinarians. In addition, chickens confined on the premises of cases 1 and 2 and without direct contact with infected cats remained healthy.

Prior reports of HPAI H5N1 infection in domestic cats document acute infections, with naturally infected cats dying within 1–4 days after disease onset [8,10] and experimental infections of unvaccinated cats terminating by 7 days post infection [9,10,12,13,15]. In other circumstances, the disease duration was unknown [4]. To the authors' knowledge, this report is novel in that it describes a domestic cat with HPAI H5N1 encephalitis dying 10 days after disease onset and with extensive malacic lesions (case 2). This report expands our knowledge of the range of lesions of HPAI H5N1 infection in domestic cats and supports findings that endothelial damage, vasculitis and vascular thrombosis are also important features of its pathogenesis.

Funding

This work was partially financed with startup funds through the University of Nebraska-Lincoln Veterinary Diagnostic Center.

Acknowledgments

We thank the National Veterinary Services Laboratories for providing virus sequences and analysis, in particular Dr Kris Lantz and Mary Lea Killian. We thank Dr Kelly Bockmann, Dr Bailee Bang and Dr Brad Johnson for their assistance with sample collection and reporting of clinical findings for these cases. Special thanks to Dr J. Dustin Loy for his technical review of this manuscript. The authors

greatly appreciate the technicians and staff of the Veterinary Diagnostic Center for their diligent work and contributions to processing these cases.

Declaration of competing interests

The authors declared no conflicts of interest in relation to the research, authorship or publication of this article.

Appendix A. Supplementary data

Supplementary data to this article can be found online at https://doi.org/10.1016/j.jcpa.2023.07.001.

References

[1] Centers for Disease Control and Prevention. Bird flu current situation summary. https://www.cdc.gov/flu/avianflu/avian-flu-summary.htm [Accessed 12 April 2023.]
[2] Caliendo V, Lewis NS, Pohlmann A, Baillie SR, Banyard AC, Beer M, et al. Transatlantic spread of highly pathogenic avian influenza H5N1 by wild birds from Europe to North America in 2021. Sci Rep 2022;12(1):11729.
[3] Puryear W, Sawatzki K, Hill N, Foss A, Stone JJ, Doughty L, et al. Highly pathogenic avian influenza A(H5N1) virus outbreak in New England seals, United States. Emerg Infect Dis 2023;29(4):786–91.
[4] Klopfleisch R, Wolf PU, Uhl W, Gerst S, Harder T, Starick E, et al. Distribution of lesions and antigen of highly pathogenic avian influenza virus A/Swan/Germany/R65/06 (H5N1) in domestic cats after presumptive infection by wild birds. Vet Pathol 2007;44(3):261–8. https://doi.org/10.1354/vp.44-3-261.
[5] Lee K, Lee EK, Lee H, Heo GB, Lee YN, Jung JY, et al. Highly pathogenic avian influenza A(H5N6) in domestic cats, South Korea. Emerg Infect Dis 2018;24(12):2343–7.
[6] Bevins SN, Shriner SA, Cumbee Jr JC, Dilione KE, Douglass KE, Ellis JW, et al. Intercontinental movement of highly pathogenic avian influenza A(H5N1) clade 2.3.4.4 virus to the United States, 2021. Emerg Infect Dis 2022;28(5):1006–11.
[7] Horimoto T, Gen F, Murakami S, Iwatsuki-Horimoto K, Kato K, Hisasue M, et al. Cats as a potential source of emerging influenza virus infections. Virol Sin 2015;30(3):221–3.
[8] Songserm T, Amonsin A, Jam-on R, Sae-Heng N, Meemak N, Pariyothorn N, et al. Avian influenza H5N1 in naturally infected domestic cat. Emerg Infect Dis 2006;12(4):681–3.
[9] Kuiken T, Rimmelzwaan G, van Riel D, van Amerongen G, Baars M, Fouchier R, et al. Avian H5N1 influenza in cats. Science 2004;306(5694):241.
[10] Rimmelzwaan GF, van Riel D, Baars M, Bestebroer TM, van Amerongen G, Fouchier RAM, et al. Influenza A virus (H5N1) infection in cats causes systemic disease with potential novel routes of virus spread within and between hosts. Am J Pathol 2006;168(1):176–83.
[11] Youk S, Torchetti MK, Lantz K, Lenoch JB, Killian ML, Leyson C, et al. H5n1 highly pathogenic avian influenza clade 2.3.4.4b in wild and domestic birds: introductions into the United States and reassortments, December 2021–April 2022. Available at SSRN 4477349, https://doi.org/10.2139/ssrn.4477349.
[12] Reperant LA, van de Bildt MW, van Amerongen G, Leijten LM, Watson S, Palser A, et al. Marked endotheliotropism of highly pathogenic avian influenza virus H5N1 following intestinal inoculation in cats. J Virol 2012;86(2):1158–65.
[13] Kim HM, Park EH, Yum J, Kim HS, Seo SH. Greater virulence of highly pathogenic H5N1 influenza virus in cats than in dogs. Arch Virol 2015;160(1):305–13.
[14] Carvallo FR, Stevenson VB. Interstitial pneumonia and diffuse alveolar damage in domestic animals. Vet Pathol 2022;59(4):586–601.
[15] Vahlenkamp TW, Harder TC, Giese M, Lin F, Teifke JP, Klopfleisch R, et al. Protection of cats against lethal influenza H5N1 challenge infection. J Gen Virol 2008;89:968–74.